Journal of Biomolecular NMR, **18:** 83–100, 2000.
KLUWER/ESCOM

Lipari–Szabo mapping: A graphical approach to Lipari–Szabo analysis of NMR relaxation data using reduced spectral density mapping

Michael Andrec[a,b,*], Gaetano T. Montelione[a,c] & Ronald M. Levy[b]
[a]*Center for Advanced Biotechnology and Medicine,* [b]*Department of Chemistry, Wright-Rieman Laboratories, and* [c]*Department of Molecular Biology and Biochemistry, Rutgers, The State University of New Jersey, Piscataway, NJ 08854-8087, U.S.A.*

Received 8 May 2000; Accepted 27 July 2000

Key words: cold-shock protein A, CspA, protein dynamics

Abstract

In this paper, we explore connections between the Lipari–Szabo formalism and reduced spectral density mapping, and show how spectral density estimates can be associated with Lipari–Szabo parameters via a simple geometric construction which we call Lipari–Szabo mapping. This relationship can be used to estimate Lipari–Szabo parameters from spectral density estimates without the need for nonlinear optimization, and to perform 'model selection' in a graphical manner. The Lipari–Szabo map also provides insight into the Lipari–Szabo model, and allows us to determine when a given set of experimental spectral densities are inconsistent with the Lipari–Szabo formalism. Practical applications of Lipari–Szabo mapping in conjunction with more traditional analysis methods are discussed.

Abbreviations: CspA, cold-shock protein A; CSA, chemical shift anisotropy.

Introduction

Dynamics play a significant role in the biological functions of proteins and other macromolecules (McCammon and Harvey, 1987; Brooks et al., 1988; Jardetzky, 1996), and NMR relaxation is a powerful tool for the study of molecular motion in these molecules (Levy and Keepers, 1986; Palmer, 1997; Fischer et al., 1998). As molecular motions are stochastic processes, they can be described in terms of a time correlation function $C(t)$. Observable NMR relaxation rates can then be expressed as functions of $C(t)$ or more conveniently, the spectral density function $J(\omega)$, which is simply the Fourier transform of $C(t)$ and describes the frequency content of the motion experienced by a given spin or spin pair (Fischer et al., 1998). The dependence of relaxation rates on $J(\omega)$ for various relaxation mechanisms is well known (Cavanagh et al., 1996; Fischer et al., 1998). For example, in an isolated heteronuclear spin pair (^{1}H and ^{15}N for the purposes of this paper) subject only to dipole-dipole and chemical shift anisotropy (CSA) relaxation mechanisms, the longitudinal relaxation rate R_1, the transverse relaxation rate R_2, and the heteronuclear cross-relaxation rate R_x (obtained experimentally from the steady-state heteronuclear NOE) of the ^{15}N spin are given by linear combinations of $J(\omega)$ evaluated at $\omega = 0$, ω_N, $\omega_H - \omega_N$, ω_H, and $\omega_H + \omega_N$. Thus, a description of the motions experienced by a heteronuclear spin pair in the form of the time-correlation or spectral density function provides sufficient information to predict the heteronuclear relaxation rates. However, the inverse problem of learning about the motions from knowledge of the relaxation rates is much more difficult. First of all, it is not possible to define the shape of a function (e.g., the spectral density) based on a finite number of experimental measurements, unless we assume some model for the function which contains

*To whom correspondence should be addressed at: Department of Chemistry, Rutgers, The State University of New Jersey, 610 Taylor Road, Piscataway, NJ 08854-8087, U.S.A. E-mail: andrec@lutece.rutgers.edu

a finite number of adjustable parameters less than or equal to the number of measurements. Furthermore, even a fully determined spectral density function may not contain sufficient information to establish the nature of the physical motion, since very different motional processes can lead to indistinguishable spectral densities (Lipari and Szabo, 1982).

Since only a finite number of points on the $J(\omega)$ curve contribute to the experimentally observable relaxation, one could avoid the use of any model by estimating only those values of $J(\omega)$ which contribute to the experimental data, rather than trying to estimate the entire functional form of $J(\omega)$. These values would then constitute a quantitative model-independent description of the spectral density funtion resulting from the motion experienced by an internuclear vector, including the overall tumbling of the molecule and any internal motions that may be present. This strategy, known as spectral density mapping, was first proposed by Peng and Wagner (Peng and Wagner, 1992b). Their original approach, however, was made cumbersome by the fact that the three commonly measured relaxation rates (R_1, R_2, and R_x) are insufficient to uniquely determine the five spectral density values ($J(0)$, $J(\omega_N)$, $J(\omega_H)$, and $J(\omega_H \pm \omega_N)$), and experiments to measure other relaxation rates, such as those of two spin order and antiphase coherences, had to be devised. More recently, the spectral density mapping approach has since been reformulated assuming that $J(\omega_H-\omega_N) \approx J(\omega_H) \approx J(\omega_H+\omega_N)$, or that $J(\omega) \propto \omega^{-2}$ for large ω, thereby reducing the number of unknowns from five to three (the so-called 'reduced spectral density mapping' method) (Farrow et al., 1995; Ishima and Nagayama, 1995). Since R_1, R_2, and R_x are linear functions of $J(\omega)$, one can obtain the $J(\omega)$ values by solving a system of linear algebraic equations, making the analysis mathematically very straightforward (Fischer et al., 1998). Unfortunately, the resulting $J(\omega)$ values cannot be easily visualized in terms of a physical description of the motion, especially since they represent a superposition of information about the internal and overall motional degrees of freedom.

In order to obtain a physical description of the internal motion, most analyses of NMR relaxation data assume some functional form for $J(\omega)$, the adjustable parameters of which have an intuitive physical meaning. One can imagine many physically reasonable models for the motion experienced by a particular internuclear vector (such as n-site jump or diffusion in a cone), and expressions for $C(t)$ have been derived for a number of such models (Daragan and Mayo, 1997). As mentioned above, there is usually not enough information in the rather limited number of noise-corrupted relaxation data typically measured to unambiguously reject all but one possible physical model. This difficulty prompted Lipari and Szabo to develop a functional form for $J(\omega)$ which contains a minimal number of adjustable parameters and which does not depend on the assumption of a precise physical model for its validity (Lipari and Szabo, 1982). This formalism, known as the 'model-free' approach, has proved to be extremely popular for the analysis of NMR relaxation data (Palmer, 1997; Fischer et al., 1998).

In this paper, we explore the relationship between the Lipari–Szabo formalism and reduced spectral density mapping. Based on this relationship, we show how the spectral density estimates can be associated with Lipari–Szabo parameters via a simple geometric construction, which we call Lipari–Szabo mapping. This graphical procedure compares the location of experimentally estimated spectral densities relative to a parametric curve representing the spectral densities for a single Lorentzian. We show how the Lipari–Szabo mapping can be used to perform 'model selection' (the decision whether contributions from conformational exchange or multiple timescale motions must be invoked to fit the data for a given residue), and determine when a given set of experimental spectral densities are inconsistent with the Lipari–Szabo formalism. Previously, we proposed a graphical approach for visualizing the uncertainty of the Lipari–Szabo parameters based on a direct propagation of the experimental uncertainties (Jin et al., 1997, 1998). However, that method was limited to the case where there was no conformational exchange or multiple timescale motions. The Lipari–Szabo mapping method addresses this deficiency. It is our belief that the detailed quantitative study of macromolecular dynamics via NMR relaxation requires more than three relaxation data per residue as well as more powerful, statistically rigorous analysis methods (Andrec et al., 1999, 2000). Lipari–Szabo mapping is intended as a means of better understanding the information content of the three commonly measured NMR relaxation data (R_1, R_2, and NOE at one field strength), as a method for quickly evaluating whether or not such relaxation data for a particular residue can be fit using the Lipari–Szabo formalism at a given overall tumbling correlation time, and as a supplement to existing software for the analysis of these data.

Theory and methods

In the Lipari–Szabo model-free formalism, the spectral density function for the motion of a given bond vector is given by

$$J(\omega) = \frac{2}{5}\left[\frac{S^2\tau_m}{1+\omega^2\tau_m^2} + \frac{(1-S^2)\tau}{1+\omega^2\tau^2}\right], \quad (1)$$

where S^2 is a measure of the spatial restriction of the internal motion, τ_e is a measure of the timescale of the internal motion, τ_m is the rotational correlation time for the overall isotropic tumbling, and $\tau^{-1} = \tau_e^{-1} + \tau_m^{-1}$ (Lipari and Szabo, 1982). If the internal motion is very rapid (i.e. in the 'extreme narrowing limit'), then τ_e approaches zero, whereas if there is no internal motion, then S^2 is unity. It has been found that not all protein ^{15}N NMR relaxation data can be fit well to a spectral density of the form of Equation 1. In particular, it is sometimes necessary to account for chemical exchange effects by adding an exchange contribution $R_{ex} = \omega_N^2\Phi_{ex}$ to the predicted R_2, where ω_N is the Larmor frequency of ^{15}N and Φ_{ex} is a constant that depends on the chemical shift differences, populations, and interconversion rates for the exchanging species (Fischer et al., 1998). Furthermore, it is sometimes necessary to invoke motion on two widely separated time scales to adequately fit the data, resulting in the so-called 'extended model-free approach' of Clore et al. (1990):

$$J(\omega) = \frac{2}{5}S_f^2\left[\frac{S_s^2\tau_m}{1+\omega^2\tau_m^2} + \frac{(1-S_s^2)\tau}{1+\omega^2\tau^2}\right], \quad (2)$$

where S_s^2 is the order parameter for the slow motion, S_f^2 is the order parameter for the fast motion, and τ_e is the effective correlation time for the slow motion (the fast motion is assumed here to be in the extreme narrowing limit). It is possible, however, that some experimental data cannot be fit even using these extensions.

We will assume that three experimental relaxation measurements at a single field strength (R_1, R_2, and heteronuclear steady-state NOE) are available, and that their uncertainties are described by uncorrelated normal probability densities with means μ_1, μ_2, μ_N, and standard deviations σ_1, σ_2, σ_N, respectively. Since the spectral density values are linearly related to R_1, R_2, and the cross-relaxation rate R_x, it is first necessary to estimate R_x from the experimental R_1 and NOE measurements using the relation

$$R_x = (\gamma_N/\gamma_H)(\mathrm{NOE}-1)R_1, \quad (3)$$

where γ_N and γ_H are the gyromagnetic ratios of ^{15}N and ^{1}H, respectively (Fischer et al., 1998). The uncertainty in R_x is then given by the probability density of the product of the two normally distributed random variables x and y, where $x = (\gamma_N/\gamma_H)(NOE-1)$ has mean (γ_N/γ_H) $(\mu_N - 1)$ and standard deviation $|\gamma_N/\gamma_H|$ σ_N and $y = R_1$ has mean μ_1 and standard deviation σ_1. Although the probability density of R_x in general cannot be written in closed form (Craig, 1936), it can be well-approximated by a normal density with mean

$$\mu_x = (\gamma_N/\gamma_H)(\mu_N - 1)\mu_1, \quad (4)$$

and standard deviation

$$\sigma_x = \left|\frac{\gamma_N}{\gamma_H}\right|\sqrt{\sigma_N^2\mu_1^2 + \sigma_1^2(\mu_N-1)^2} \quad (5)$$

determined using traditional 'propagation of errors' (Bevington, 1969) if $P(x)$ and $P(y)$ do not have appreciable density at $x = 0$ or $y = 0$. In that limit, we also find that there is minimal correlation between R_1 and R_x.

In the reduced spectral density mapping method, the relationship between the relaxation rates R_1, R_2, and R_x and the spectral density is given by the linear system

$$\mathbf{A}\,\mathbf{j} = \mathbf{d}, \quad (6)$$

where $\mathbf{j} = (J(0)\ J(\omega_N)\ J(0.87\ \omega_H))^T$, $\mathbf{d} = (R_1\ R_2\ R_x)^T$,

$$\mathbf{A} = \begin{pmatrix} 0 & b & 7a \\ \frac{2}{3}b & \frac{1}{2}b & \frac{13}{2}a \\ 0 & 0 & 5a \end{pmatrix} \quad (7)$$

$$a = \left(\frac{\mu_0 h\gamma_H\gamma_N}{16\pi^2 r_{NH}^3}\right)^2, \quad b = 3a + \frac{(\omega_N\Delta\sigma)^2}{3}, \quad (8)$$

μ_0 is the permeability of free space, h is the Planck constant, r_{NH} is the mean N–H bond length, and $\Delta\sigma$ is the magnitude of the CSA for ^{15}N. For a ^{1}H field strength of 500 MHz, $r_{NH} = 1.02$ Å, and $\Delta\sigma = -160$ ppm, we obtain $a \approx 1.2985$ and $b \approx 4.762$ for **j** in units of ns/rad and **d** in units of Hz. For notational convenience, we will represent the three spectral density values in Equation 6 as $J_0 \equiv J(0)$, $J_N \equiv J(\omega_N)$, and $J_H \equiv J(0.87\omega_H)$. The estimation of the value and uncertainty of **j** given the value and uncertainty of **d** is a linear problem, and its solution is particularly simple, especially if viewed from a Bayesian perspective

(Sivia, 1996), where we can summarize the information about the spectral density values in the form of a posterior probability density function. In the case of a uniform prior density over **j** the posterior probability density of **j** is given by a multivariate normal density with mean

$$\boldsymbol{\mu}_j = \left(\mathbf{A}^T \Sigma_d^{-1} \mathbf{A}\right)^{-1} \mathbf{A}^T \Sigma_d^{-1} \mathbf{d} \tag{9}$$

and covariance matrix

$$\Sigma_j = \left(\mathbf{A}^T \Sigma_d^{-1} \mathbf{A}\right)^{-1}, \tag{10}$$

where

$$\Sigma_{\mathbf{d}} = \begin{pmatrix} \sigma_1^2 & 0 & 0 \\ 0 & \sigma_2^2 & 0 \\ 0 & 0 & \sigma_x^2 \end{pmatrix} \tag{11}$$

is the covariance matrix describing the uncertainty in the relaxation data (Ó Ruanaidh and Fitzgerald, 1996). Thus, the uncertainty in **j** can be estimated directly via Equation 10 without the need for Monte Carlo error estimation methods.

In keeping with the semi-quantitative spirit of this paper, we will approximate the uncertainty in **j** by a box with sides parallel to the J_0, J_N, and J_H axes centered at μ_j and having widths equal to $3(\Sigma_j)_{ii}^{1/2}$ (1.5 standard deviations about the mean). We will further assume that all **j** values inside this box are feasible (i.e. have equal and finite posterior probabilities), and those outside are not (i.e., have posterior probability zero). Since the diagonal elements of Σ_j represent the variances of the marginal densities of each element of **j**, this box represents a conservative estimate of the uncertainty in **j**. Of course, one could more rigorously represent the uncertainty as a smooth function or as ellipsoidal confidence bounds; however, we believe that a box representation of the uncertainty is not unrealistic and more appropriate for the purposes of this paper. In general, the neglect of statistical correlations among the spectral densities will tend to overestimate the uncertainties in our analyses. If accurate quantitative uncertainty estimates are required, we recommend the use of more rigorous statistical parameter estimation methods (Andrec et al., 1999, 2000). It should be noted, however, that all of the theoretical relationships between Lipari–Szabo parameters and spectral density values derived below are rigorous. On the other hand, the derivation of spectral density values from experimental relaxation data and their uncertainties are correct only to within the approximation of reduced spectral density mapping, and the estimates of uncertainties in the Lipari–Szabo parameters and 'model selections' based on those estimates are valid only to within the box-function approximation of the uncertainty in **j**. For demonstration purposes, we will make use of ^{15}N relaxation data for the major cold-shock protein from *Escherichia coli* (CspA) (Table 1), for which a standard analysis performed using the MODELFREE software package (Mandel et al., 1995) has been published (Feng et al., 1998).

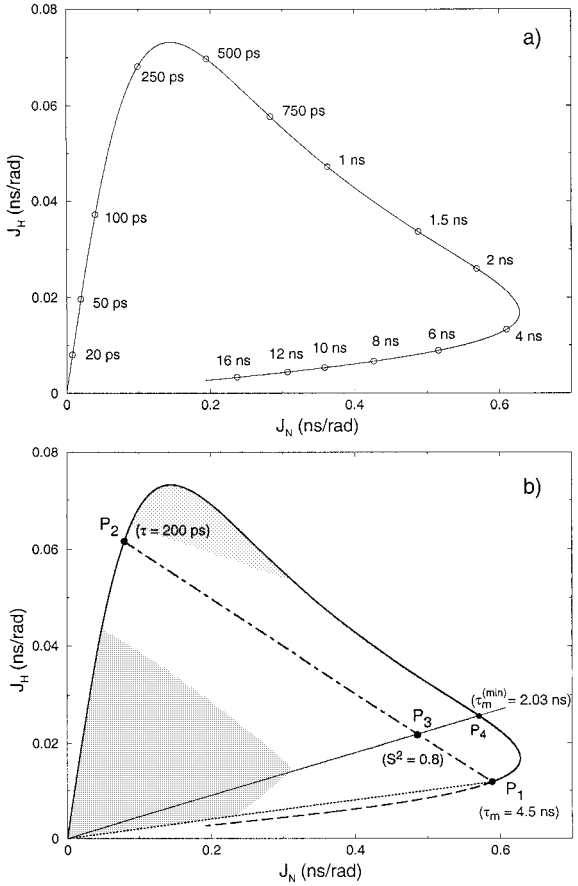

Figure 1. (a) The parametric curve $(J_N^{(\text{rigid})}(t),\ J_H^{(\text{rigid})}(t))$ corresponding to all possible (J_N, J_H) points consistent with rigid isotropic tumbling (Equation 12). The circles are labeled with the values of t corresponding to that point on the curve. The curve continues to approach the origin as t approaches infinity. (b) The shaded region indicates the (J_N, J_H) points consistent with internal motions described by Equation 1 or 2 for an overall tumbling correlation time of 4.5 ns. Point P_1 represents the (J_N, J_H) point for Equation 1 with $\tau_m = 4.5$ ns and $S^2 = 1$. Point P_2 represents the (J_N, J_H) point for Equation 1 with $\tau = 200$ ps and $S^2 = 0$. The line segment connecting P_1 and P_2 represents the (J_N, J_H) points consistent with Equation 1 with $\tau_m = 4.5$ ns, $\tau = 200$ ps and $0 < S^2 < 1$. Point P_3 represents the (J_N, J_H) point for Equation 1 with $\tau_m = 4.5$ ns, $\tau = 200$ ps and $S^2 = 0.8$. Point P_4 represents the (J_N, J_H) point corresponding to the smallest possible τ_m consistent with point P_3 (for which τ_e and τ would be zero).

Table 1. Relaxation data, spectral density estimates, and MODELFREE parameter estimates for the selected residues of CspA shown in Figures 3 and 7

Residue number	Relaxation data (R_1, R_2, NOE)[a]	Spectral density estimates (J_0, J_N, J_H)[b]	MODELFREE parameter estimates[c]			
			S^2 (or S_s^2)[d]	τ_c (ps)	R_{ex} (s^{-1})	S_f^2
29	2.16 ± 0.08 6.57 ± 0.08 0.72 ± 0.07	1.72 ± 0.03 0.44 ± 0.02 0.009 ± 0.002	0.77 ± 0.03	0	0.71 ± 0.24	1
36	2.68 ± 0.12 7.08 ± 0.14 0.70 ± 0.09	1.79 ± 0.05 0.54 ± 0.03 0.012 ± 0.004	0.92 ± 0.02	$105 \pm -$[e]	0	1
41	2.21 ± 0.07 4.57 ± 0.06 0.29 ± 0.04	1.06 ± 0.02 0.42 ± 0.02 0.025 ± 0.002	0.69 ± 0.02	232 ± 56	0	0.86 ± 0.02
42	2.07 ± 0.10 5.68 ± 0.10 0.35 ± 0.07	1.44 ± 0.04 0.39 ± 0.02 0.021 ± 0.002	0.71 ± 0.01	142 ± 38	0	1
46	1.93 ± 0.10 8.33 ± 0.17 0.13 ± 0.05	2.29 ± 0.06 0.36 ± 0.02 0.026 ± 0.002	0.58 ± 0.02	288 ± 89	3.58 ± 0.22	1
57	2.37 ± 0.22 5.75 ± 0.16 0.52 ± 0.09	1.42 ± 0.06 0.46 ± 0.05 0.018 ± 0.004	0.74 ± 0.02	93 ± 45	0	1
69	2.27 ± 0.15 6.12 ± 0.13 0.70 ± 0.09	1.56 ± 0.05 0.46 ± 0.03 0.011 ± 0.003	0.80 ± 0.02	0	0	1

[a]Relaxation rates (in s^{-1}) and steady state NOE values and their uncertainties ($\pm$ 1 standard deviation) measured by Feng et al. (1998).
[b]Spectral density values (in ns/rad) and their uncertainties ($\pm$ 1 standard deviation) estimated using Equations 4–11.
[c]Lipari–Szabo parameter estimates reported by Feng et al. (1998) using a τ_m estimate of 4.88 ns.
[d]Reported value is S^2 (Equation 1) if $S_f^2 = 1$, otherwise the reported value is S_s^2 (Equation 2).
[e]Error estimate could not be determined reliably from previous statistical analysis (Feng et al., 1998).

Results

Relationship between reduced spectral density mapping and the simple Lipari–Szabo model

In order to investigate the relationship between Equation 1 and the results of reduced spectral density mapping, let us first consider the family of possible (J_N, J_H) values for rigid isotropic tumbling (i.e., the single Lorentzian of Equation 1 with $S^2 = 1$). This is given by the parametric curve ($J_N^{(rigid)}(t)$, $J_H^{(rigid)}(t)$) for $0 \leq t < \infty$ (Figure 1a), where

$$J_i^{(rigid)}(t) = \frac{2}{5}\frac{t}{1+\omega_i^2 t^2} \qquad (12)$$

As can be seen in Figure 1a, this curve is approximately triangle-shaped, with the three sides corresponding to the regimes of $\omega t \ll 1$, $\omega t \approx 1$, and $\omega t \gg 1$. Thus, if experimental (J_N, J_H) spectral density values coincide with this curve to within experimental error, then the data are consistent with rigid tumbling for some value of τ_m. It is much more likely, however, that the experimental (J_N, J_H) values do not coincide with this curve due to the effects of internal motion. Let us next consider the family of (J_N, J_H) values consistent with Equation 1 for a given value of τ_m and τ ($\tau^{-1} = \tau_e^{-1} + \tau_m^{-1}$), and all possible values of S^2. Substituting into Equation 1, we find that this is

given by the parametric curve

$$\begin{cases} J_{\mathrm{N}} = S^2\left(J_{\mathrm{N}}^{(\mathrm{rigid})}(\tau_m) - J_{\mathrm{N}}^{(\mathrm{rigid})}(\tau)\right) \\ \qquad +J_{\mathrm{N}}^{(\mathrm{rigid})}(\tau) \\ \qquad\qquad\qquad\qquad 0 \le S^2 \le 1. \\ J_{\mathrm{H}} = S^2\left(J_{\mathrm{H}}^{(\mathrm{rigid})}(\tau_m) - J_{\mathrm{H}}^{(\mathrm{rigid})}(\tau)\right) \\ \qquad +J_{\mathrm{H}}^{(\mathrm{rigid})}(\tau) \end{cases} \quad (13)$$

Equating the two parts of Equation 13 after solving for S^2, we find that the curve of Equation 13 is equivalent to

$$\frac{J_{\mathrm{H}} - J_{\mathrm{H}}^{(\mathrm{rigid})}(\tau)}{J_{\mathrm{H}}^{(\mathrm{rigid})}(\tau_m) - J_{\mathrm{H}}^{(\mathrm{rigid})}(\tau)} = \frac{J_{\mathrm{N}} - J_{\mathrm{N}}^{(\mathrm{rigid})}(\tau)}{J_{\mathrm{N}}^{(\mathrm{rigid})}(\tau_m) - J_{\mathrm{N}}^{(\mathrm{rigid})}(\tau)}, \quad (14)$$

which is simply the equation for the straight line in the (J_{N}, J_{H}) plane passing through the points $P_1 = (J_{\mathrm{N}}^{(\mathrm{rigid})}(\tau_m), J_{\mathrm{H}}^{(\mathrm{rigid})}(\tau_m))$ and $P_2 = (J_{\mathrm{N}}^{(\mathrm{rigid})}(\tau), J_{\mathrm{H}}^{(\mathrm{rigid})}(\tau))$, as shown in Figure 1b. Comparison with Equation 1 shows that points P_1 and P_2 simply represent the contributions from the $\tau_m/(1 + \omega^2\tau_m^2)$- and $\tau/(1 + \omega^2\tau^2)$-containing terms of the Lipari–Szabo spectral density, respectively. As S^2 varies from 1 to 0, the spectral densities move along this line from P_1 to P_2, and the ratio of the distance between a given point on the line and P_2 to the distance between P_1 and P_2 is equal to the value of S^2. Changes in the internal correlation time τ_e result in the movement of point P_2 along the 'rigid tumbling' curve from the origin (for $\tau_e = \tau = 0$) to P_1 ($\tau_e \to \infty$). Furthermore, it is apparent that the set of all possible (J_{N}, J_{H}) values consistent with Equation 1 for an independently determined value of τ_m consists of the region below the 'rigid tumbling' curve and above the line passing through P_1 and the origin (corresponding to $\tau_e = 0$) and is indicated by the gray region in Figure 1b. It is also apparent that for very large τ_e values (such that τ approaches τ_m) the P_1-P_2 distance becomes quite short, and large changes in S^2 result in correspondingly smaller changes in J_{N} and J_{H}. Thus, uncertainties in S^2 are much larger when τ_e is large for equivalent J_{N} and J_{H} uncertainties, as has been demonstrated previously using other methods (for example, Jin et al., 1998). The linear relationship of Equation 14 is clearly not specific to ω_{N} and ω_{H}, but is true for spectral densities evaluated at any pair of frequencies when Equation 1 is valid (with $R_{\mathrm{ex}} = 0$), as has been noted previously (Lefèvre et al., 1996; Guenneugues et al., 1999). Furthermore, such a linear relationship also exists for the relaxation rates R_1, R_2, and R_x, as has been pointed out previously by Fushman et al. (1994). In principle, one could recast all of the results in this paper in terms of correlations between the observed relaxation rates and those predicted by rigid tumbling, however the resulting equations would be considerably more cumbersome (cf. Appendix).

In the above construction, it was assumed that an independent estimate of τ_m is available. However, knowledge of an experimental (J_{N}, J_{H}) point allows us to establish a lower bound on τ_m that is independent of any such estimate. This minimum τ_m corresponds to the value of t at which the 'rigid tumbling' curve ($J_{\mathrm{N}}^{(\mathrm{rigid})}(t)$, $J_{\mathrm{H}}^{(\mathrm{rigid})}(t)$) intersects the line passing through the given (J_{N}, J_{H}) point and the origin (i.e., $\tau_e = 0$) (point P_4 in Figure 1), and corresponds to the case of a single Lorentzian in Equation 1. Its value is given by

$$\tau_m^{(\mathrm{min})} = \sqrt{\frac{J_{\mathrm{N}} - J_{\mathrm{H}}}{J_{\mathrm{H}}\omega_{\mathrm{H}}^2 - J_{\mathrm{N}}\omega_{\mathrm{N}}^2}}. \quad (15)$$

In most cases, this bound will be of little practical use, as it will almost always be less than ≈ 3 ns (the t value corresponding to the second 'corner' in the curve of Figure 1a). However, it will be seen below that $\tau_m^{(\mathrm{min})}$ is also numerically equal to the maximum possible value of τ consistent with a (J_{N}, J_{H}) point if we allow $S_f^2 \neq 1$, and this will play an important role in understanding the feasible ranges of the extended Lipari–Szabo parameters.

The above geometric construction relating Lipari–Szabo parameters to a point in the (J_{N}, J_{H}) plane also allows us to calculate the values of S^2 and τ_e in Equation 1 consistent with a given (J_{N}, J_{H}) point and a given value of τ_m without the need for nonlinear optimization or any other iterative numerical method. Consider a point $P_{\mathrm{obs}} = P_3 = (J_{\mathrm{N}}^{(\mathrm{obs})}, J_{\mathrm{H}}^{(\mathrm{obs})})$ in the gray region in Figure 1b. To find what values of S^2 and τ are consistent with P_{obs} at the given value of τ_m, we first construct the line through P_{obs} and $P_1 = (J_{\mathrm{N}}^{(\mathrm{rigid})}(\tau_m), J_{\mathrm{H}}^{(\mathrm{rigid})}(\tau_m))$, which is given by

$$J_{\mathrm{H}} = cJ_{\mathrm{N}} + d, \quad (16)$$

where

$$c = \frac{J_{\mathrm{H}}^{(\mathrm{rigid})}(\tau_m) - J_{\mathrm{H}}^{(\mathrm{obs})}}{J_{\mathrm{N}}^{(\mathrm{rigid})}(\tau_m) - J_{\mathrm{N}}^{(\mathrm{obs})}}$$

and

$$d = J_{\mathrm{H}}^{(\mathrm{rigid})}(\tau_m) - cJ_{\mathrm{N}}^{(\mathrm{rigid})}(\tau_m).$$

The value of τ corresponds to the point at which the line of Equation 16 intersects the 'rigid tumbling' curve, i.e., it is a root of the equation

$$cJ_N^{(rigid)}(\tau) + d = J_H^{(rigid)}(\tau).$$

Expanding and collecting terms, we find that

$$\begin{aligned}&(\tfrac{5}{2}c^{-1}d\omega_H^2\omega_N^2)\tau^4 + (\omega_H^2 - \omega_N^2c^{-1})\tau^3 \\ &+(\tfrac{5}{2}c^{-1}d\omega_H^2\omega_N^2)\tau^2 + (1 - c^{-1})\tau + \tfrac{5}{2}c^{-1}d = 0,\end{aligned} \quad (17)$$

which is a quartic equation in τ. However, we know (by construction) that one of the roots of this equation must be $\tau = \tau_m$. Dividing the left-hand side of Equation 17 by $(\tau - \tau_m)$, we obtain finally the cubic equation

$$\tau^3 + A\tau^2 + B\tau + C = 0, \quad (18)$$

where

$$A = \frac{5(J_N^{(obs)}\omega_N^2k_N - J_H^{(obs)}\omega_H^2k_H) + 2\tau_m(\omega_H^2 - \omega_N^2)}{5\omega_H^2\omega_N^2\tau_m(J_H^{(obs)}k_H - J_N^{(obs)}k_N)},$$

$$B = \frac{5(J_H^{(obs)}\omega_N^2k_H - J_N^{(obs)}\omega_H^2k_N) + 2\tau_m(\omega_H^2 - \omega_N^2)}{5\omega_H^2\omega_N^2(J_H^{(obs)}k_H - J_N^{(obs)}k_N)},$$

$$C = \frac{-1}{\omega_H^2\omega_N^2\tau_m},$$

and

$$k_i = 1 + \omega_i^2\tau_m^2.$$

A numerical solution for the real root(s) of Equation 18 can be obtained using a closed-form, noniterative method (Press et al., 1992). Once τ has been found, we can locate $P_2 = (J_N^{(rigid)}(\tau), J_H^{(rigid)}(\tau))$, as well as convert τ into τ_e using the relation

$$\tau_e = \frac{\tau_m\tau}{\tau_m - \tau}. \quad (19)$$

The value of S^2 can then be calculated from

$$S^2 = \frac{d(P_{obs}, P_2)}{d(P_1, P_2)}, \quad (20)$$

where $d(\ )$ is the Euclidean distance between two points in the (J_N, J_H) plane. Since the presence of chemical exchange contributes only to J_0 (see below), the solution outlined above remains valid whether or not $R_{ex} = 0$. Therefore, it is possible to determine the values of S^2 and τ_e in a direct, noniterative manner without the need to explicitly estimate R_{ex}. As mentioned above, one could make use of the linear relationship between R_1 and R_x to construct a polynomial in τ analogous to Equation 18 above which would be immune to any inaccuracies arising from the reduced spectral density mapping approximation. However, such a strategy results in a sixth-order polynomial which cannot be solved in a noniterative manner (see Appendix).

Mapping of J_0 information onto the (J_N, J_H) plane and 'model selection'

Thus far, we have only made use of the values of J_N and J_H. In this section, we show below how to incorporate J_0 information into the J_N vs J_H plot described above to create the full 'Lipari–Szabo map'. It will be seen below that this is critical, since the detection of deviations from simple Lipari–Szabo behavior requires the simultaneous analysis of J_0, J_N, and J_H information. For the moment, however, let us assume that Equation 1 (with $R_{ex} = 0$) is valid for a given residue and that J_0 is known precisely. Given values for J_0, τ, and τ_m, we can solve Equation 1 for S^2:

$$S^2 = \frac{\frac{5}{2}J_0 - \tau}{\tau_m - \tau} \quad (21)$$

Equation 21 specifies a curve (an 'iso-J_0 contour') through (S^2, τ) space as a function of $\tau(0 \le \tau \le \frac{5}{2}J_0)$ which gives a constant value of J_0 when substituted into Equation 1 with a given τ_m. One can readily convert Equation 21 into an equivalent iso-J_0 contour in the (J_N, J_H) plane, as shown in Figure 2. As can be seen there, the iso-J_0 contours move closer to the point $P_1 = (J_N^{(rigid)}(\tau_m), J_H^{(rigid)}(\tau_m))$ as J_0 increases, and vice versa. We can determine the consistency of the data with Equation 1 simply by plotting the experimental J_N and J_H spectral densities together with the iso-J_0 contour for the experimental J_0 spectral density. If the experimental (J_N, J_H) point coincides with the iso-J_0 contour to within experimental error, then the data can be fit with Equation 1 to within experimental error. Otherwise, the data are not consistent with Equation 1, and additional adjustable parameters must be used to adequately fit the data. Of course, since the representation of the uncertainties in the spectral densities as a box is only approximate, this method cannot be used as a statistically rigorous hypothesis test. However, it can still be usefully employed as an addition to existing analysis software to identify possible model-selection ambiguities independently of more formal statistical tests, as will be seen below, especially since this approach is so well suited to graphical representation.

As an example of the Lipari–Szabo mapping approach to 'model selection', we have generated

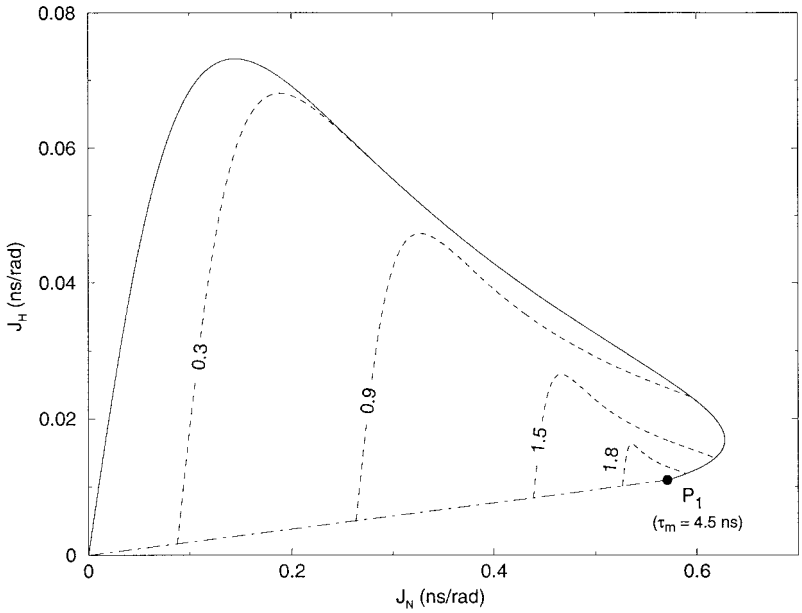

Figure 2. The 'rigid tumbling' curve (solid line), point $P_1 = (J_N^{(\mathrm{rigid})}(\tau_m), J_H^{(\mathrm{rigid})}(\tau_m))$ for $\tau_m = 4.5$ ns (filled circle), and the '$\tau_e = 0$ line' for $\tau_m = 4.5$ ns (dot-dashed line), together with the 'iso-J_0 contours' (Equation 21) for $J_0 = 0.3$, 0.9, 1.5, and 1.8 ns/rad (dashed lines).

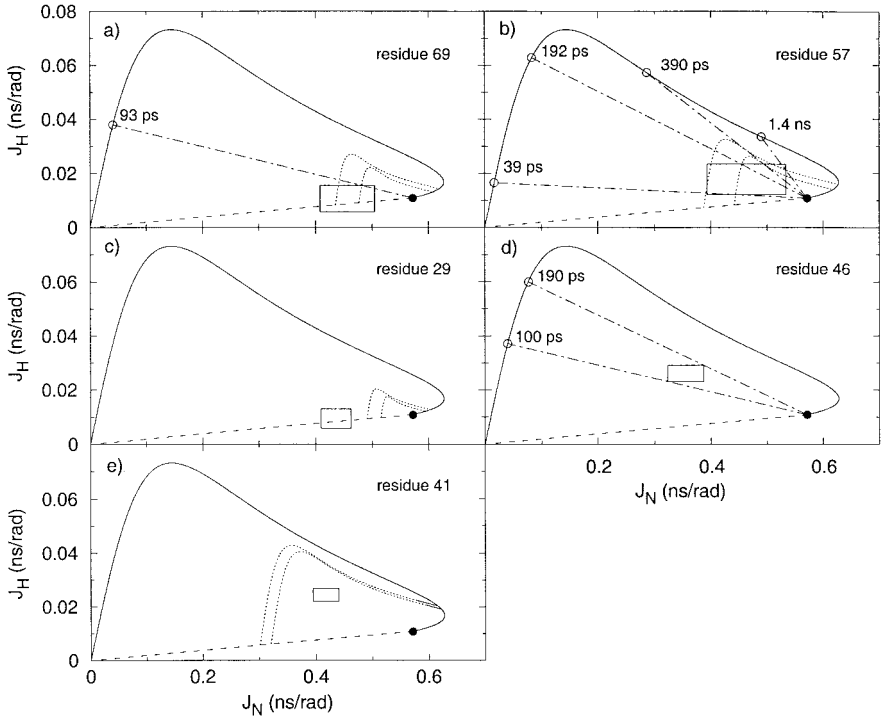

Figure 3. Lipari–Szabo maps for selected residues of the *E. coli* major cold-shock protein CspA (Feng et al., 1998). The final τ_m estimate obtained by Feng et al. (4.88 ns) is used throughout. The dotted lines correspond to the iso-J_0 contours for $J_0 \pm 1.5\sigma$, and the rectangles represent $J_N \pm 1.5\sigma$ and $J_H \pm 1.5\sigma$ as estimated using Equations 9–10. The dot-dashed lines correspond to upper or lower bounds on τ determined by the spectral density estimates.

Lipari–Szabo maps for several residues of CspA (Feng et al., 1998), assuming $\tau_m = 4.88$ ns and isotropic tumbling (Figure 3). The spectral densities and their uncertainties were estimated using Equations 9 and 10 as described above. The Lipari–Szabo map for residue 69 (Figure 3a) demonstrates that the J_N and J_H estimates are consistent with $\tau_e = 0$, since the rectangle representing the uncertainties in J_N and J_H overlaps the line passing through $P_1 = (J_N^{(rigid)}(\tau_m), J_H^{(rigid)}(\tau_m))$ and the origin. Furthermore, the J_N and J_H estimates are consistent with Equation 1, since the iso-J_0 contours corresponding to the minimum and maximum J_0 values overlap the (J_N, J_H) uncertainty box. This result agrees with the MODELFREE model selection result (Table 1). It is clear from Figure 3a, however, that τ values as large as ≈ 90 ps are still consistent with the spectral density estimates, since such τ values will still give rise to P_1-P_2 lines which intersect both the (J_N, J_H) uncertainty box and the region between the upper and lower bound iso-J_0 contours. If we assume that $\tau_e = 0$, then the feasible range of S^2 is determined completely by the feasible range of J_0, since both the maximum and minimum iso-J_0 contours lie inside the (J_N, J_H) box for $\tau_e = 0$. Using the feasible range defined by $\pm 1.5\sigma$, i.e., $1.49 \leq J_0 \leq 1.64$ ns/rad, we find from Equation 1 a feasible range for the order parameter of $0.76 \leq S^2 \leq 0.84$, which is in excellent agreement with the $\pm 1.5\sigma$ bounds of $0.77 \leq S^2 \leq 0.83$ determined using MODELFREE (Table 1).

The J_N and J_H spectral density estimates for residue 57 (Figure 3b), on the other hand, are clearly not consistent with $\tau_e = 0$, since the rectangle representing the uncertainties in J_N and J_H does not overlap the line passing through $P_1 = (J_N^{(rigid)}(\tau_m), J_H^{(rigid)}(\tau_m))$ and the origin. The iso-J_0 contours indicate that the spectral densities are still consistent with Equation 1; however, their curvature results in two distinct regions of (S^2, τ) space consistent with the data: one with $40 \leq \tau \leq 190$ ps and the other with 390 ps $\leq \tau \leq 1.4$ ns. Only the former region was reported in the MODELFREE analysis (Table 1). The presence of two disjoint feasible (S^2, τ) regions is confirmed using our previously described graphical analysis method (Jin et al., 1997) (Figure 4); however, the estimated ranges of τ differ slightly. This may be a result of the box-function approximation to the posterior probability of **j** used in the present analysis or of a failure of the reduced spectral density mapping approximation.

Detection and estimation of R_{ex} contributions

Residue 29 (Figure 3c) is an example where the spectral densities are not consistent with Equation 1. In particular, the J_N and J_H spectral densities are similar to those of residue 69 (Figure 3a) in that they are consistent with $\tau_e = 0$. However, the J_0 estimates are clearly larger than would be expected based on the observed J_N and J_H if Equation 1 were valid. This can be seen in Figure 3c by noting that the iso-J_0 contours do not overlap the (J_N, J_H) feasible region, but are shifted closer to the point $P_1 = (J_N^{(rigid)}(\tau_m), J_H^{(rigid)}(\tau_m))$. As has been noted previously (Peng and Wagner, 1995), the presence of an R_{ex} contribution to the transverse relaxation rate will result in an inflated J_0 value while leaving the other spectral densities unchanged, since J_0 contributes only to R_2 (Equations 6–7). The magnitude of R_{ex} can therefore be estimated by calculating the apparent J_0 value that would result in an iso-J_0 contour that passes through the observed (J_N, J_H) point ($J_0^{(app)}$). The value of R_{ex} is then related to the 'excess' J_0 and is given by

$$R_{ex} = \tfrac{2}{3} b (J_0^{(obs)} - J_0^{(app)}), \qquad (22)$$

where the constant b is the same as in Equation 8 (Fushman et al., 1994; Peng and Wagner, 1995). For residue 29, the feasible range for S^2 is determined completely by the uncertainty in J_N if we assume that $\tau_e = 0$, and is given by $0.72 \leq S^2 \leq 0.82$, which agrees very well with the $\pm 1.5\sigma$ range estimated using MODELFREE ($0.73 \leq S^2 \leq 0.82$). The range of $J_0^{(app)}$ values consistent with this range of S^2 can be found by substituting into Equation 1, and is given by $1.41 \leq J_0^{(app)} \leq 1.60$ ns/rad. Taken together with the upper and lower bounds on the observed J_0 in Table 1, we estimate the feasible range for R_{ex} using Equation 22 to be $0.25 \leq R_{ex} \leq 1.14$ s^{-1} (compared to $0.35 \leq R_{ex} \leq 1.07$ s^{-1} MODELFREE estimate). It is apparent from this analysis that values of S^2 and τ can be estimated from the observed (J_N, J_H) values without the need to estimate the value of R_{ex}. This does not imply, however, that S^2 and τ are uncorrelated with R_{ex}, since points within the feasible (J_N, J_H) region further away from $P_1 = (J_N^{(rigid)}(\tau_m), J_H^{(rigid)}(\tau_m))$ which correspond to smaller values of S^2 will result in larger estimates of R_{ex}.

The situation is even more dramatic for residue 46 (Figure 3d), where the observed J_0 value is larger than the maximum possible value for $\tau_m = 4.88$ ns (equal to $\frac{2}{5}\ \tau_m = 1.95$ ns/rad). In this case, the iso-J_0 contours are undefined and therefore they do not

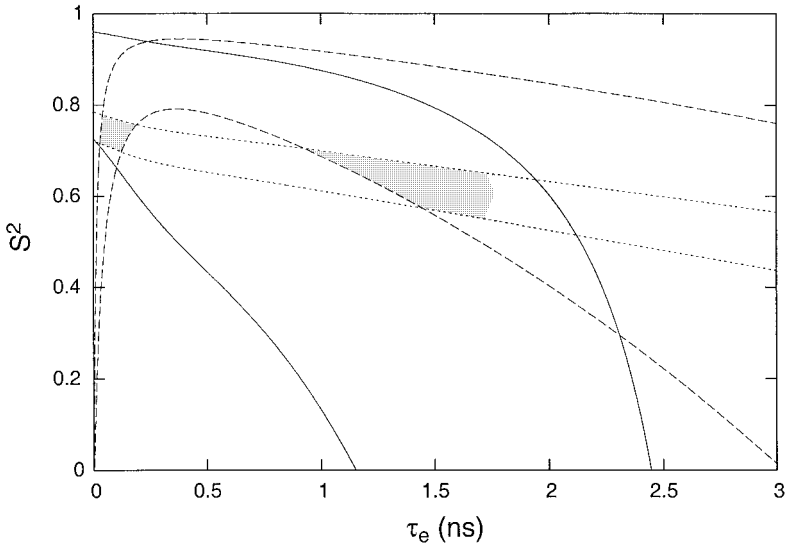

Figure 4. Results of the Jin et al. graphical method of Lipari–Szabo error propagation (Jin et al., 1997, 1998) for residue 57 of CspA calculated using $\tau_m = 4.88$ ns. The curves correspond to contours of constant R_1 (solid lines), R_2 (dotted lines), and NOE (dashed lines) for the observed data ± 1.5 standard deviation. The region between each pair of curves corresponds to the set of (S^2, τ_e) points consistent with that datum. The intersection of those sets (shown in gray) are those values of S^2 and τ_e consistent with all of the data. The upper and lower bounds on τ_e are given by $30 \leq \tau_e \leq 190$ ps and $0.9 \leq \tau_e \leq 2.1$ ns for the two disjoint feasible regions (corresponding to τ ranges of $30 \leq \tau \leq 180$ ps and $0.8 \leq \tau \leq 1.5$ ns, respectively).

appear in Figure 3d at all. The bounds on J_N and J_H clearly preclude $\tau_e = 0$, and since in this case the J_0 estimate provides no information that would restrict the feasible range of S^2 and τ_e, the feasible (J_N, J_H) range provides an immediate estimate of lower and upper bounds on τ_e of $100 \leq \tau_e \leq 190$ ps (Figure 3d), compared to the MODELFREE estimate of $150 \leq \tau_e \leq 420$ ps. Since the iso-J_0 contours form a monotonically increasing surface as we approach $P_1 = (J_N^{(\text{rigid})}(\tau_m),\ J_H^{(\text{rigid})}(\tau_m))$ (Figure 2), the maximum and minimum values of $J_0^{(\text{app})}$ consistent with the (J_N, J_H) box must lie on the edge of the box. In this case, they correspond to the lower right and upper left corners of the (J_N, J_H) box and are given by $1.04 \leq J_0^{(\text{app})} \leq 1.28$ ns/rad. From this we can use Equation 22 to obtain a feasible range for R_{ex} of $2.92 \leq R_{ex} \leq 4.25\ \text{s}^{-1}$, which is somewhat larger than, though generally consistent with, the MODELFREE result of $3.25 \leq R_{ex} \leq 3.91\ \text{s}^{-1}$.

Detection and estimation of multiple timescale motion

The 'extended model-free approach' of Clore et al. (1990), which was devised to fit more complex motions occurring on multiple timescales, contains an additional order parameter (S_f^2, Equation 2) compared to the simple Lipari–Szabo model. If we allow S_s^2 to play the same role as S^2 in the above analysis, then allowing $S_f^2 \neq 1$ simply has the effect of moving a point in (J_N, J_H)-space that is consistent with Equation 1 along a straight line toward the origin (since Equations 1 and 2 differ only by the overall scaling factor S_f^2). Such a translation obviously cannot move a (J_N, J_H) point outside of the shaded region of Figure 1b. Thus, all (J_N, J_H) points consistent with Equation 2 are also consistent with Equation 1 for different values of the internal motional parameters, and vice versa. Therefore, the determination that the extended Lipari–Szabo model is required to fit the data to within experimental uncertainty can be done only via a simultaneous analysis of J_0, J_N, and J_H.

Knowledge of J_N and J_H alone, however, is sufficient to determine upper and lower bounds to τ, as well as a lower bound to S_f^2. Consider a point in the interior of the feasible (J_N, J_H) region (say, point P_3 in Figure 5a). To be consistent with this point, S_s^2 and τ must be chosen such that the values

$$J'_N = \frac{2}{5}\left[\frac{S_s^2\tau_m}{1+\omega_N^2\tau_m^2} + \frac{(1-S_s^2)\tau}{1+\omega_N^2\tau^2}\right]$$
and
$$J'_H = \frac{2}{5}\left[\frac{S_s^2\tau_m}{1+\omega_H^2\tau_m^2} + \frac{(1-S_s^2)\tau}{1+\omega_H^2\tau^2}\right] \quad (23)$$

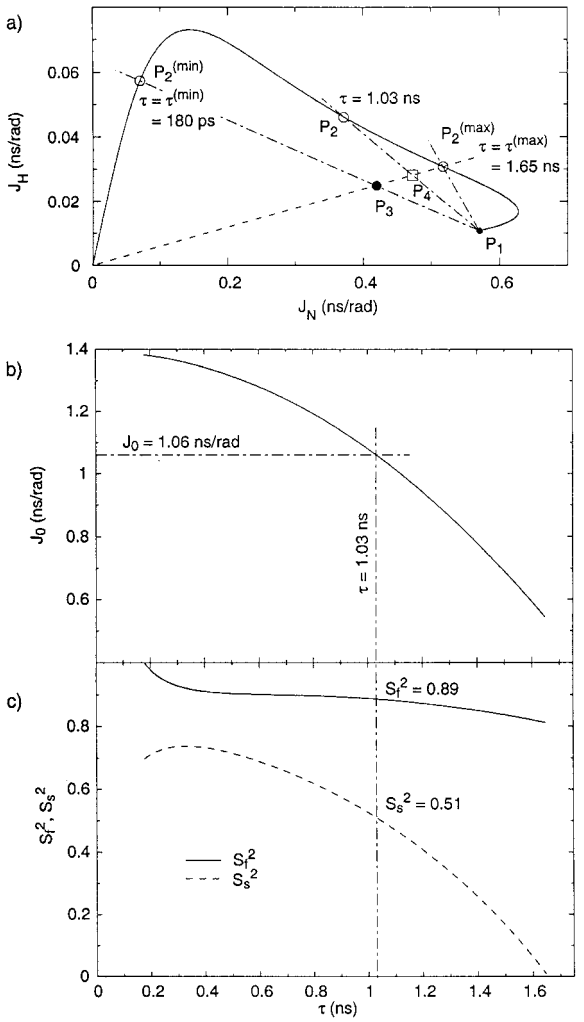

Figure 5. (a) A Lipari–Szabo mapping approach to finding the family of (S_s^2, τ, S_f^2) values consistent with a given (J_N, J_H) point P_3. As described in the text, one can set the value of τ to anything in the range $\tau^{(min)} \leq \tau \leq \tau^{(max)}$ ($P_2^{(min)}$ to $P_2^{(max)}$) and still find values of S_s^2 and S_f^2 that will give spectral densities consistent with point P_3 when substituted into Equation 2. The intersection of the line passing through $P_1 = (J_N^{(rigid)}(\tau_m), J_H^{(rigid)}(\tau_m))$ and $P_2 = (J_N^{(rigid)}(\tau), J_H^{(rigid)}(\tau))$ for any feasible value of t with the line passing through $P_2^{(max)}$ and the origin (point P_4) can be used to determine those values of S_s^2 and S_f^2. In this case, P_1 corresponds to $\tau_m = 4.88$ ns, and P_3 corresponds to the observed J_N and J_H values for residue 41 of CspA (0.42 and 0.025 ns/rad, respectively). (b) A curve showing J_0 as τ increases from $\tau^{(min)}$ to $\tau^{(max)}$ (i.e., as P_2 moves from $P_2^{(min)}$ to $P_2^{(max)}$). (c) The corresponding values of S_s^2 and S_f^2 determined from point P_4. The dot-dashed lines in (b) and (c) illustrate the determination of the S_s^2, S_f^2, and t values consistent with the observed value of J_0 for residue 41 of CspA (1.06 ns/rad).

lie on the line passing through P_3 and the origin, and between P_3 and the 'rigid tumbling' curve (i.e., between points P_3 and $P_2^{(max)}$ in Figure 5a), since for any such (J'_N, J'_H) point (e.g., point P_4 in Figure 5a) one can find a value of S_f^2 ($0 \leq S_f^2 \leq 1$) that will bring this point into coincidence with the observed point P_3. Point P_4 can lie on the line segment between P_3 and $P_2^{(max)}$ only if the value of τ lies in the interval between $\tau^{(min)}$ (corresponding to $S_f^2 = 1$ and represented graphically by point $P_2^{(min)}$ determined from P_3 and $P_1 = (J_N^{(rigid)}(\tau_m), J_H^{(rigid)}(\tau_m))$) and $\tau^{(max)}$ (corresponding to $S_f^2 = 0$ and represented graphically by point $P_2^{(max)}$), where $\tau^{(max)}$ is numerically equal to the $\tau_m^{(min)}$ of Equation 15. Furthermore, since the 'rigid tumbling' curve establishes an upper bound on J'_N and J'_H, this determines a lower bound on S_f^2, given by

$$S_f^2(\text{min}) = \frac{J_N}{J_N^{(rigid)}(\tau^{(max)})} = \frac{J_H}{J_H^{(rigid)}(\tau^{(max)})}. \quad (24)$$

This lower bound corresponds to the single-Lorentzian limit of $S_s^2 = 0$ in Equation 2, and it depends only on the relative positions of P_3 and $P_2^{(max)}$ and not on the values of J_0 or τ_m. Moving P_3 closer to the origin increases the magnitude of the 'upper bound' J'_N and J'_H values relative to the J_N and J_H values of P_3, and reduces the lower bound on S_f^2, approaching a limiting value of zero as P_3 approaches the origin.

Thus, the set of all possible values of S_s^2, τ, and S_f^2 consistent with a given point in the (J_N, J_H) plane (point P_3 in Figure 5a) can be constructed by allowing τ to vary from its minimum to its maximum value (i.e., from points $P_2^{(min)}$ to $P_2^{(max)}$) and finding the intersection of the line between ($J_N^{(rigid)}(\tau_m)$, $J_H^{(rigid)}(\tau_m)$) and ($J_N^{(rigid)}(\tau)$, $J_H^{(rigid)}(\tau)$) and the line between P_3 and $P_2^{(max)}$ (e.g., point P_4). However, the value of J_0 calculated from those S_s^2, τ, and S_f^2 and Equation 2 is not constant, as can be seen in Figure 5b: J_0 is at its maximum value for the minimum value of τ, and decreases monotonically as τ increases and S_f^2 decreases, reaching a minimum at the maximum value of τ. This lower bound on J_0 given by

$$J_0^{(min)} = \tfrac{2}{5} S_f^2(\text{min}) \tau^{(max)}, \quad (25)$$

where S_f^2(min) is given by Equation 24. If the estimated J_0 value is smaller than $J_0^{(min)}$ for the observed J_N and J_H values, then it can be concluded that the

data are not consistent with the Lipari–Szabo spectral density of the form of Equation 1 or Equation 2 for any value of τ_m (since $S_f^2(\text{min})$ and $\tau^{(\text{max})}$ are both independent of τ_m).

If the estimated J_0 value is larger than $J_0^{(\text{min})}$ but smaller than the J_0 value that would be expected based on Equation 1 and the observed (J_N, J_H) point (to within experimental error), then it can be concluded that $S_f^2 \neq 1$ is required to fit the data. One can solve for the S_s^2, S_f^2, and τ values consistent with a (J_0, J_N, J_H) point and a given value of τ_m simply by finding the value of τ for which the curve of Figure 5b intersects the observed J_0 value. Although we cannot construct a non-iterative method for the determination of t along the lines of Equation 18, it can be readily estimated using a one-dimensional root-finding algorithm (Press et al., 1992). Once τ has been found, S_s^2 can be determined from points P_1, P_2, and P_4 in analogy to Equation 20, and S_f^2 is the constant needed to make P_4 coincident with P_3 (Figures 5a and 5c). Error estimation is more difficult in this case, since changes in J_N or J_H will cause a shift in the curve of J_0 vs τ. However, since the dependence of J_0 on τ is smooth and monotonic, numerical estimation of τ will be very efficient and robust. The values of S_s^2 and S_f^2 can be found in closed form, and a simple Monte Carlo procedure can be used to reliably estimate the uncertainties in the motional parameters.

As an example of this in the context of real data, consider the spectral density estimates for residue 41 of CspA. The Lipari–Szabo map for this residue (Figure 3e) indicates that the observed J_0 value is smaller than what would be expected based on the observed J_N and J_H, since the iso-J_0 contours lie further away from the point $P_1 = (J_\text{N}^{(\text{rigid})}(\tau_m), J_\text{H}^{(\text{rigid})}(\tau_m))$ than the feasible (J_N, J_H) region. From the intersection of the J_0 vs τ curve of Figure 5b with the observed value $J_0 = 1.06$ ns/rad we find that the spectral densities for residue 41 can be fit exactly by Equation 2 with $\tau = 1.03$ ns, $S_s^2 = 0.51$, and $S_f^2 = 0.89$ at the estimated τ_m of 4.88 ns (giving $\tau_e = 1.31$ ns). This differs significantly from the MODELFREE estimates of $\tau_e = 232$ ps, $S_s^2 = 0.69$, and $S_f^2 = 0.86$. Back-calculation of the relaxation rates using the exact expressions (Fischer et al., 1998) using the MODELFREE parameters and those estimated here shows that the latter are a better fit: the MODELFREE parameters give $R_1 = 1.93\ \text{s}^{-1}$, $R_2 = 4.80\ \text{s}^{-1}$, and NOE = 0.21 ($\chi^2 = 34.7$), while the parameters estimated here give $R_1 = 2.21\ \text{s}^{-1}$, $R_2 = 4.57\ \text{s}^{-1}$, and NOE = 0.27 ($\chi^2 = 0.25$). Clearly, the nonlinear fitting procedure used previously did not succeed in finding the least-squares fit. Although the parameters estimated here do fit the spectral densities exactly, they do not fit the relaxation data exactly (i.e., $\chi^2 = 0.25 > 0$). This is likely due to the quantitative failure of the reduced spectral density mapping approximation, and is particularly apparent in the NOE datum, which is dominated by $J(\omega_\text{H} \pm \omega_\text{N})$ and therefore is most susceptible to such a failure. However, the deviation between the parameters estimated from Lipari–Szabo mapping and the exact fit parameters determined by direct nonlinear optimization ($\tau = 1.05$ ns, $S_s^2 = 0.51$, and $S_f^2 = 0.88$) is quite small, and is likely to be negligible compared to the uncertainties arising from experimental uncertainties in the relaxation rates.

Although the 'model selection' methods used in software such as MODELFREE (Mandel et al., 1995) make use of classical statistical hypothesis tests which cannot compare models with equal numbers of parameters (Jin et al., 1998), in the particular case of testing between models with $R_\text{ex} \neq 0$ and those with $S_f^2 \neq 1$ this limitation is not a severe shortcoming. The need for either $R_\text{ex} \neq 0$ or $S_f^2 \neq 1$ is determined by whether the observed J_0 value is significantly larger or smaller than what would be expected based on the observed J_N and J_H values. It obviously cannot be both, and as long as τ_m is known and remains constant there can be no ambiguity between 'model 4' (S^2, τ, R_ex, $S_f^2 = 1$) and 'model 5' (S_s^2, τ, $R_\text{ex} = 0$, S_f^2), unless the data are already well fit by 'model 2' (S^2, τ, $R_\text{ex} = 0$, $S_f^2 = 1$) (in the nomenclature of Mandel et al., 1995). Of course, this does not logically preclude the possibility that $R_\text{ex} \neq 0$ *and* $S_f^2 \neq 1$, in which case the parameter estimate is underdetermined if only three relaxation data have been measured. We consider this case in the following section.

Mapping of the (S_s^2, τ, R_ex, S_f^2) nullspace in an underdetermined system

If we are willing to consider the possibility that a given residue could have both $R_\text{ex} \neq 0$ and $S_f^2 \neq 1$, then the parameter estimate is obviously underdetermined if only R_1, R_2, and NOE measurements at one field strength have been made. Ideally, this situation should be addressed by the collection of more data to unambiguously determine the parameter values, as we have advocated (Andrec et al., 1999). However, if the collection of more data is impossible or impractical, then it is still possible to determine bounds on the mo-

tional parameters even for an underdetermined system. The extraction of useful information from underdetermined models (also known as 'ill-posed inverse problems') is certainly not without precedent in NMR spectroscopy or the physical sciences in general. Such models arise routinely in geophysics, for example, where unique solutions are often obtained by imposing additional 'regularization' criteria (Tarantola, 1987). One common regularization method familiar to NMR spectroscopists is the 'maximum entropy' criterion, which has been used to select a unique high digital resolution frequency-domain representation of lower digital resolution time-domain data (Stephenson, 1988). However, for many ill-posed problems there exist physical constraints which can significantly limit the size of the possible solution space even in the absence of any regularization criteria (for a recent NMR-related example, see Losonczi and Prestegard, 1998). We demonstrate here that the Lipari–Szabo model itself provides such constraints, and that these constraints can be used to determine upper and/or lower bounds on the motional parameters.

In our case, the (J_0, J_N, J_H) values define a one-dimensional curve (known as the 'nullspace') through the (S_s^2, τ, R_{ex}, S_f^2) parameter space which fit the data exactly (assuming $J_0 \geq J_0^{(min)}$ and no experimental uncertainty). For linear problems, the nullspace is a linear subspace of the parameter space, and a set of orthonormal basis vectors for the nullspace can be easily determined using singular value decomposition (Press et al., 1992). For a nonlinear model (such as the one considered here), the nullspace consists of a nonlinear subspace of the parameter space, and in general cannot be expressed in closed form. In our case, however, we can make use of the Lipari–Szabo mapping procedure to numerically estimate and plot the curve corresponding to the nullspace for any set of (J_0, J_N, J_H) data (with $J_0 \geq J_0^{(min)}$). In fact, this curve is simply a generalization of the curve already seen in Figure 5b. Suppose that for residue 41 of CspA we wish to consider the possibility that both $R_{ex} \neq 0$ and $S_f^2 \neq 1$, and we again assume that the spectral densities for residue 41 are given by (J_0, J_N, J_H) = (1.06, 0.42, 0.025) with no experimental uncertainty. It is clear from the above arguments that S_f^2 cannot equal 1, but must be at most 0.89, since any larger value would lead to a predicted J_0 which is larger than that observed. On the other hand, values of S_f^2 less than 0.89 are now feasible, since they lead to predicted J_0 values which are smaller than those observed, and the 'excess' J_0 can be attributed to an R_{ex} contribution. However, we know that there is a lower bound on the apparent J_0 that is independent of the observed J_0 and corresponds to the limit $S_s^2 = 0$. This, in turn, implies an upper bound on R_{ex}, given by

$$R_{ex}^{(max)} = \tfrac{2}{3} b (J_0 - J_0^{(min)}). \qquad (26)$$

In the case of CspA residue 41, $R_{ex}^{(max)}$ is equal to 1.66 s^{-1}. As above, the effect of uncertainty on the motional parameters is difficult to express analytically, but can easily be determined via simple Monte Carlo and presented graphically as a 'scatter plot' of nullspace curves, as shown in Figure 6. Thus, for the general underdetermined fit of S_s^2, τ, R_{ex}, and S_f^2 to J_0, J_N, and J_H, we can obtain nontrivial upper and lower bounds on τ, a lower bound in S_f^2 (and a nontrivial upper bound if the data cannot be fit with $S_f^2 = 1$), an upper bound on R_{ex} (and a nontrivial lower bound if the data cannot be fit with $R_{ex} = 0$), and an upper bound on S_s^2 (the lower bound always being $S_s^2 = 0$). These limits can be seen in the 'scatter plot' of Figure 6 as the bounds enclosing the entire 'bundle' of curves.

Discussion

The mapping of spectral density estimates and the geometric relationship between those estimates and the Lipari–Szabo parameters provides many useful insights into both the information content of the spectral density estimates as well as the Lipari–Szabo model. In addition to providing approximate parameter estimates and 'model selections' as described above, Lipari–Szabo mapping can also be used to detect cases which might give rise to pathologies in the parameter estimation or ambiguities in the 'model selection'. This is illustrated with two examples from the CspA data set in Figure 7. In general, the closer the feasible (J_N, J_H) region is to the point $P_1 = (J_N^{(rigid)}(\tau_m), J_H^{(rigid)}(\tau_m))$, the larger will be the uncertainty in τ_e, reaching the extreme case of infinite uncertainty if P_1 is inside the feasible (J_N, J_H) region. Figure 7a shows the results for residue 36 of CspA, and it is immediately apparent that the point P_1 for $\tau_m = 4.88$ does in fact lie inside the (J_N, J_H) feasible region. As a consequence, it is not possible to establish an upper or lower bound on τ_e for this residue, and for large values of τ_e this will result in very large uncertainties in S_2 as discussed above. Feng et al. did in fact

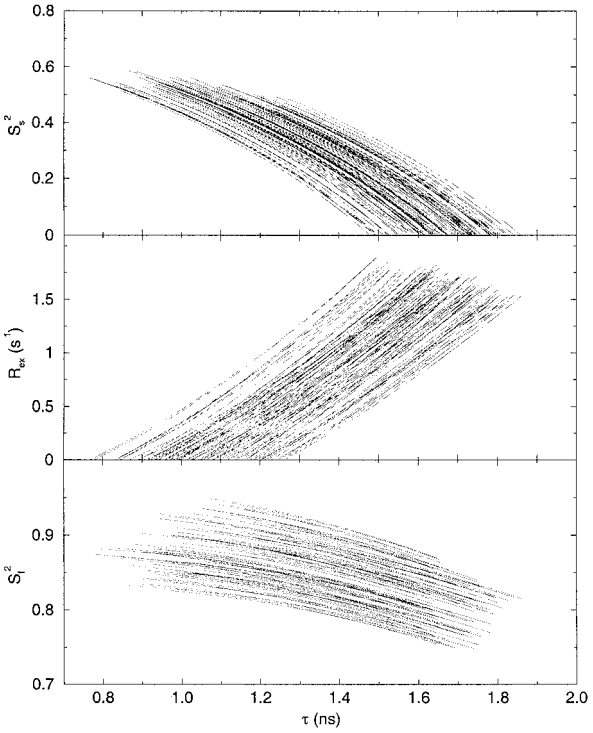

Figure 6. A 'scatter plot' of curves corresponding to the nonlinear nullspace associated with the underdetermined fit of S_s^2, τ, R_{ex}, and S_f^2 to J_0, J_N, and J_H for the spectral densities and uncertainties of residue 41 of CspA (using $\tau_m = 4.88$ ns). One hundred points uniformly distributed in the feasible (J_0, J_N, J_H) region estimated using Equations 9–10 were generated, and the four-dimensional curve corresponding to the (S_s^2, τ, R_{ex}, S_f^2) nullspace for each point was determined. The projections of that family of curves onto the S_s^2 vs τ, R_{ex} vs τ, and S_f^2 vs τ planes are shown. Taken together, these represent the 'tube' through (S_s^2, τ, R_{ex}, S_f^2)-space that is consistent with the spectral density estimates for residue 41 of CspA.

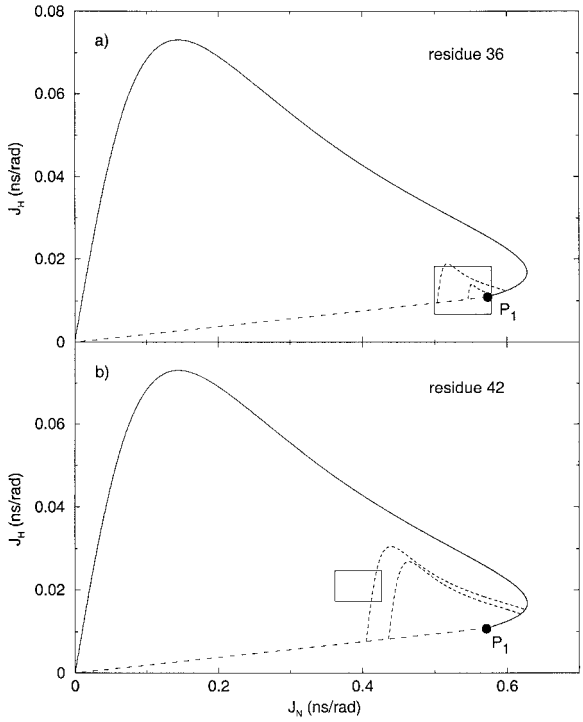

Figure 7. Lipari–Szabo maps for two residues of CspA for which Lipari–Szabo parameter estimation and 'model selection' could lead to pathologies (see Discussion). The lines, curves, and boxes have the same meanings as in Figure 3 above.

recognize the very large uncertainty in τ_e, and for that reason did not report an error estimate for that parameter (Table 1). However, this earlier estimate of the uncertainty in S_2 is likely too small, perhaps because of inadequate exploration of the parameter space by the Monte Carlo error estimation method. The results for residue 42 (Figure 7b) illustrate another potential difficulty that can arise in classical Lipari–Szabo analyses. In this case, a part of the feasible (J_N, J_H) region overlaps the region defined by the upper and lower bound iso-J_0 contours, while most of it lies outside of that region. This implies that although the data could be fit to within the estimated experimental errors with $R_{ex} = 0$ (which was the conclusion of the MODELFREE analysis), this 'model selection' may be ambiguous, and caution should be exercised in the interpretation of 'model selection' results for this residue. Alternatively, one could simply report an upper bound on R_{ex}, and not make an explicit choice as to whether R_{ex} is exactly equal to zero or not (Andrec et al., 1999).

Many of the results above implicitly assume that τ_m is known precisely. This is not normally the case, as τ_m must usually be determined from the relaxation data along with the internal motional parameters (Fischer et al., 1998; Andrec et al., 1999) and will have an associated uncertainty. Furthermore, most biological macromolecules are not spherically symmetric, and therefore their rotational diffusion cannot be described by a single rotational correlation time. However, if the deviation from spherical symmetry is not large and the internal motions are sufficiently well behaved, then the spectral density is well approximated by Equation 1 or 2 with an apparent τ_m that depends on the mean orientation of the bond vector in the molecule (Schurr et al., 1994; Brüschweiler et al., 1995; Andrec et al., 2000). Given structural information and an estimate of the approximate tensor parameters based on the relaxation data (Schurr et al., 1994; Brüschweiler et al., 1995;

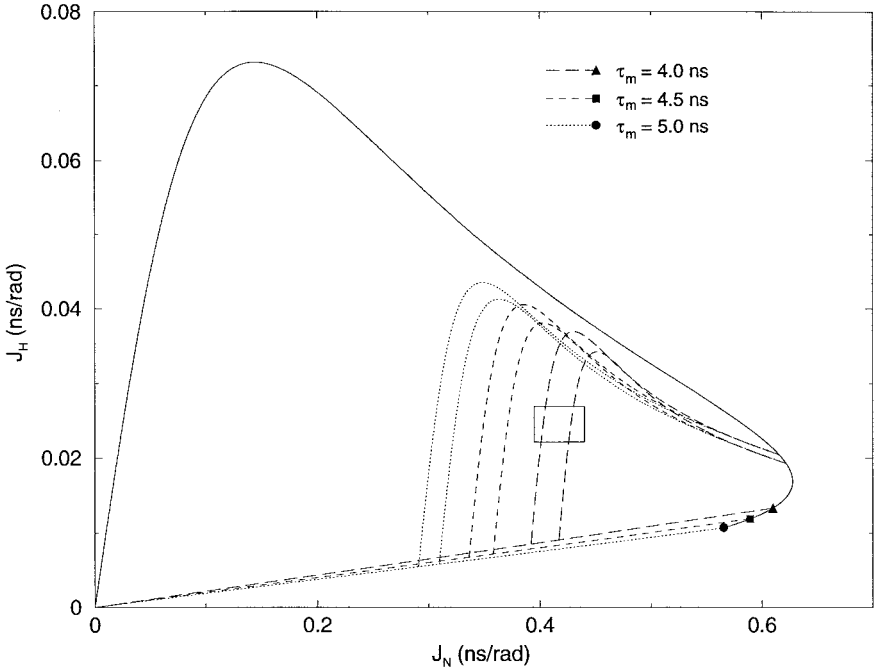

Figure 8. A superposition of three Lipari–Szabo maps for the spectral density values of residue 41 for three different values of τ_m demonstrating the effect of τ_m uncertainty on Lipari–Szabo parameter estimates and 'model selection' (see Discussion). It is clear that a change in τ_m of 0.5 ns (due to statistical uncertainty or the effects of anisotropy) can change the 'model selection' quite dramatically.

Lee et al., 1997; Clore et al., 1998), one can generate Lipari–Szabo maps where anisotropy information is encoded in apparent τ_m values.

Several general trends are immediately apparent from the geometry of the Lipari–Szabo map. First of all, given an observed (J_N, J_H) point, a decrease in τ_m will be correlated with an decrease in the estimated value of τ, as has been observed previously (Andrec et al., 1999). This correlation will be more prominent the closer the observed (J_N, J_H) point is to $P_1 = (J_N^{(\text{rigid})}(\tau_m),\ J_H^{(\text{rigid})}(\tau_m))$. Furthermore, changes in τ_m cause a shift in the iso-J_0 contour for a given value of J_0. This can result in dramatic changes in the 'model selection' as a function of τ_m, as can be seen in Figure 8. In this case, changes in the assumed τ_m of less than 500 ps result in substantial changes to the interpretation of the data: at $\tau_m = 4.0$ ns, the spectral densities are well fit by the simple Lipari–Szabo model, while at 4.5 ns they clearly require the 'extended' model. This is due primarily to the shifting of the iso-J_0 contours relative to the feasible (J_N, J_H) region as a function of τ_m.

Proponents of the spectral density mapping approach to the analysis of NMR relaxation data have argued that the method has the significant advantage that it is model-independent and more general than the Lipari–Szabo model. Lipari–Szabo mapping allows us to state precisely when the results of spectral density mapping are inconsistent with the simple or 'extended' Lipari–Szabo models (Equations 1 and 2 with or without $R_{ex} = 0$). Specifically, spectral densities can be inconsistent with the Lipari–Szabo model either because (1) J_N and J_H cannot be fit using Equation 1 or 2 irrespective of the value of J_0, or (2) J_0 cannot be fit simultaneously with J_N and J_H. Situation (1) can arise in one of two ways. The J_N and J_H values could lie outside the region of the (J_N, J_H) plane enclosed by the 'rigid tumbling' curve of Figure 1a, in which case the spectral densities cannot be fit with the Lipari–Szabo model for any value of τ_m. We conjecture that such spectral densities are also inconsistent with any physically realistic model for internal motions. Alternatively, the J_N and J_H values might lie inside the 'rigid tumbling' curve but below the '$\tau_e = 0$ line' passing through $P_1 = (J_N^{(\text{rigid})}(\tau_m),\ J_H^{(\text{rigid})}(\tau_m))$ and the origin for a given value of τ_m, or, equivalently, that $\tau_m < \tau_m^{(\text{min})}$ (Equation 15). In that case, the spectral densities cannot be fit with the Lipari–Szabo model for that value of τ_m but could be fit with a larger τ_m such that $\tau_m \geq \tau_m^{(\text{min})}$. Situation (2) can only arise if J_0 is

smaller than the $J_0^{(\min)}$ calculated using Equation 25 for the estimated values of J_N and J_H, since any other value of J_0 can be fit with an appropriate value of R_{ex} and/or S_f^2. As discussed above, such spectral densities are inconsistent with the Lipari–Szabo model of Equations 1 and 2 independent of any τ_m estimate. Any values of J_0, J_N, and J_H that do not fall into these three categories can be fit with the Lipari–Szabo model. Obviously, it is possible that relaxation data which *can* be fit by the Lipari–Szabo model could result in reduced spectral density estimates which cannot be fit by the Lipari–Szabo model due to the approximations inherent in reduced spectral density mapping.

Conclusions

We have shown that there exists a simple graphical relationship between reduced spectral density estimates and the parameters of the Lipari–Szabo model, and that one can easily obtain estimates of Lipari–Szabo parameters directly from the spectral density estimates. Furthermore, we have shown that the procedure of 'model selection' as it is currently used in Lipari–Szabo analysis can be related to the degree of internal consistency of the observed J_0, J_N, and J_H spectral densities, and that this degree of consistency can be visualized graphically. The relationship between the Lipari–Szabo model and spectral density estimates has been explored in the past (Lefèvre et al., 1996), and a method for 'model selection' based on a qualitative comparison of the relative magnitudes of J_0 and J_H has been proposed earlier (Ishima et al., 1995). This work puts that qualitative relationship on a firm quantitative footing. It also shows under what circumstances the spectral density estimates are inconsistent with the Lipari–Szabo model.

It has been suggested that the use of spectral density estimates for the study of internal motions in macromolecules is preferable to methods based on the Lipari–Szabo formalism because spectral density estimates are model-independent and are in some sense more general (Peng and Wagner, 1992a). While it is true that spectral densities are model-independent, their interpretation in terms of an intuitive physical description of the internal motions cannot be done in the absence of a model. In particular, spectral densities contain information not only about internal motions, but also about the overall tumbling of the molecule. The Lipari–Szabo formalism provides the simplest and most general method that can be used to separate those degrees of freedom assuming that they are in principle separable, and the Lipari–Szabo mapping procedure described here can be used to interpret spectral density estimates within the context of the Lipari–Szabo formalism with minimal investment in software and computing time.

Lipari–Szabo mapping requires minimal computing time, and can be used as an initial 'screening' or 'pre-processing' step prior to a more rigorous and computationally intensive analysis. In particular, it can be used to detect the presence of significant multiple minima in χ^2, as well as identify possible 'model selection' ambiguities. Given an estimate of a feasible range for τ_m (possibly making use of information from a rough estimate of the diffusion tensor parameters), it can be used to identify residues for which 'model selection' will be strongly influenced by τ_m. Furthermore, the nonlinear optimization methods used in software packages such as MODELFREE (Mandel et al., 1995) are easily trapped by local minima or strong nonlinearities, necessitating extensive grid searching to ensure that the algorithm finds a true global optimum. The methods described here could be used as a supplement or alternative to grid searching for more efficient location of good starting points for nonlinear optimization.

Appendix

We can make use of the linear relationship between R_1 and R_x (Fushman et al., 1994) to construct a polynomial in τ analogous to Equation 18 above which is immune to any inaccuracies arising from the reduced spectral density mapping approximation. We begin by noting (in analogy to Equation 16) that

$$cR_1^{(\text{rigid})}(\tau) + d = R_x^{(\text{rigid})}(\tau), \tag{A1}$$

where $R_1^{(\text{rigid})}(\tau)$ and $R_1^{(\text{rigid})}(\tau)$ are the relaxation rates corresponding to a single Lorentzian with correlation time τ, and the constants c and d are given by

$$c = \frac{R_x^{(\text{rigid})}(\tau_m) - R_x^{(\text{obs})}}{R_1^{\text{rigid}}(\tau_m) - R_1^{\text{obs})}},$$

and

$$d = R_x^{(\text{rigid})}(\tau_m) - cR_1^{(\text{rigid})}(\tau_m).$$

Expanding and collecting terms, we find that

$$\tau_6 + A\tau_5 + B\tau_4 + C\tau_3 + D\tau_2 + E\tau + F = 0, \tag{A2}$$

where

$$A = \frac{2}{5d}\left[\frac{bc}{\omega_N^2} + \frac{a(c+1)}{(\omega_H-\omega_N)^2} + \frac{6a(c-1)}{(\omega_H+\omega_N)^2}\right],$$

$$B = \omega_N^{-2} + (\omega_H-\omega_N)^{-2} + (\omega_H+\omega_N)^{-2},$$

$$C = \frac{2}{5d}\left[\frac{a(c+1)+bc}{\omega_N^2(\omega_H-\omega_N)^2} + \frac{6a(c-1)+bc}{\omega_N^2(\omega_H+\omega_N)^2} + \frac{a(7c-5)}{(\omega_H-\omega_N)^2(\omega_H+\omega_N)^2}\right],$$

$$D = \omega_N^{-2}(\omega_H-\omega_N)^{-2} + \omega_N^{-2}(\omega_H+\omega_N)^{-2} + (\omega_H-\omega_N)^{-2}(\omega_H+\omega_N)^{-2},$$

$$E = \frac{2}{5d}\frac{a(7c-5)+bc}{\omega_N^2(\omega_H-\omega_N)^2(\omega_H+\omega_N)^2},$$

and

$$F = \omega_N^{-2}(\omega_H-\omega_N)^{-2}(\omega_H+\omega_N)^{-2}.$$

The constants a and b are defined in Equation 8. Clearly, this sixth degree equation cannot be solved in a noniterative fashion. However, if one is concerned about inaccuracies due to the reduced spectral density approximation, one can determine an approximate value of τ using Equation 18, which can be used as a starting value for the numerical solution of Equation A2 using standard iterative root-finding methods (Press et al., 1992). Since the solution obtained from Equation 18 is likely to be very close to a root of Equation A2, this strategy may be more generally robust than direct nonlinear optimization of S^2 and τ_e.

Acknowledgements

We thank Gerhard Wagner for stimulating discussions concerning spectral density mapping and an anonymous reviewer for bringing to our attention the work of Fushman et al. (1994) and for other helpful suggestions. This research was supported by the National Institutes of Health (NRSA Fellowship GM19856-02 to MA, and grants GM-50733 to GTM and GM-30580 to RML). Support for CABM structural biology computing facilities was provided by a grant from the W.M. Keck Foundation.

References

Andrec, M., Inman, K.G., Weber, D.J., Levy, R.M. and Montelione, G.T. (2000) *J. Magn. Reson.*, in press.

Andrec, M., Montelione, G.T. and Levy, R.M. (1999) *J. Magn. Reson.*, **139**, 408–421.

Bevington, P.R. (1969) *Data Reduction and Error Analysis in the Physical Sciences*, McGraw-Hill, New York, NY.

Brooks, C.L., Karplus, M. and Pettit, B.M. (1988) *Proteins: A Theoretical Perspective of Dynamics, Structure, and Thermodynamics*, John Wiley & Sons, New York, NY.

Brüschweiler, R., Liao, X. and Wright, P.E. (1995) *Science*, **268**, 886–889.

Cavanagh, J., Fairbrother, W.J., Palmer, A.G. and Skelton, N.J. (1996) *Protein NMR Spectroscopy: Principles and Practice*, Academic Press, San Diego, CA.

Clore, G.M., Gronenborn, A.M., Szabo, A. and Tjandra, N. (1998) *J. Am. Chem. Soc.*, **120**, 4889–4890.

Clore, G.M., Szabo, A., Bax, A., Kay, L.E., Driscoll, P.C. and Gronenborn, A.M. (1990) *J. Am. Chem. Soc.*, **112**, 4989–4991.

Craig, C.C. (1936) *Ann. Math. Stat.*, **7**, 1–15.

Daragan, V.A. and Mayo, K.H. (1997) *Prog. NMR Spectrosc.*, **31**, 63–105.

Farrow, N.A., Zhang, O., Szabo, A., Torchia, D.A. and Kay, L.E. (1995) *J. Biomol. NMR*, **6**, 153–162.

Feng, W., Tejero, R., Zimmerman, D.E., Inouye, M. and Montelione, G.T. (1998) *Biochemistry*, **37**, 10881–10896.

Fischer, M.W.F., Majumdar, A. and Zuiderweg, E.R.P. (1998) *Prog. NMR Spectrosc.*, **33**, 207–272.

Fushman, D., Weisemann, R., Thüring, H. and Rüterjans, H. (1994) *J. Biomol. NMR*, **4**, 61–78.

Guenneugues, M., Gilquin, B., Wolff, N., Ménez, A. and Zinn-Justin, S. (1999) *J. Biomol. NMR*, **14**, 47–66.

Ishima, R. and Nagayama, K. (1995) *J. Magn. Reson.*, **B108**, 73–76.

Ishima, R., Yamasaki, K. and Nagayama, K. (1995) *J. Biomol. NMR*, **6**, 423–426.

Jardetzky, O. (1996) *Prog. Biophys. Mol. Biol.*, **65**, 171–219.

Jin, D., Andrec, M., Montelione, G.T. and Levy, R.M. (1998) *J. Biomol. NMR*, **12**, 471–492.

Jin, D., Figueirido, F., Montelione, G.T. and Levy, R.M. (1997) *J. Am. Chem. Soc.*, **119**, 6923–6924.

Lee, L.K., Rance, M., Chazin, W.J. and Palmer, A.G., III (1997) *J. Biomol. NMR*, **9**, 287–298.

Lefèvre, J.-F., Dayie, K.T., Peng, J.W. and Wagner, G. (1996) *Biochemistry*, **35**, 2674–2686.

Levy, R.M. and Keepers, J. (1986) *Commun. Mol. Cell. Biophys.*, **3**, 273–295.

Lipari, G. and Szabo, A. (1982) *J. Am. Chem. Soc.*, **104**, 4546–4559.

Losonczi, J.A. and Prestegard, J.H. (1998) *Biochemistry*, **37**, 706–716.

Mandel, A.M., Akke, M. and Palmer, A.G., III (1995) *J. Mol. Biol.*, **246**, 144–163.

McCammon, J.A. and Harvey, S. (1987) *Dynamics of Proteins and Nucleic Acids*, Cambridge University Press, Cambridge.

Ó Ruanaidh, J.J.K. and Fitzgerald, W.J. (1996) *Numerical Bayesian Methods Applied to Signal Processing*, Springer-Verlag, New York, NY.

Palmer, A.G., III (1997) *Curr. Opin. Struct. Biol.*, **7**, 732–737.

Peng, J.W. and Wagner, G. (1992a) *Biochemistry*, **31**, 8571–8586.

Peng, J.W. and Wagner, G. (1992b) *J. Magn. Reson.*, **98**, 308–332.

Peng, J.W. and Wagner, G. (1995) *Biochemistry*, **34**, 16733–16752.

Press, W.H., Teukolsky, S.A., Vetterling, W.T. and Flannery, B.P. (1992) *Numerical Recipes in C: The Art of Scientific Computing*, Cambridge University Press, Cambridge.

Schurr, J.M., Babcock, H.P. and Fujimoto, B.S. (1994) *J. Magn. Reson.*, **B105**, 211–224.
Sivia, D.S. (1996) *Data Analysis: A Bayesian Tutorial*, Oxford University Press, Oxford.
Stephenson, D.S. (1988) *Prog. NMR Spectrosc.*, **20**, 515–626.
Tarantola, A. (1987) *Inverse Problem Theory: Methods for Data Fitting and Model Parameter Estimation*, Elsevier, Amsterdam.